Aalto University

Aaltodoc
OPEN ACCESS

This is an electronic reprint of the original article.
This reprint may differ from the original in pagination and typographic detail.

Author(s):   Zubiaga, A. & Reurings, F. & Tuomisto, Filip & Plazaola, F. & Garcia, J. A. & Kuznetsov, A. Yu. & Egger, W. & Zuniga-Perez, J. & Munoz-Sanjose, V.

Title: On the interplay of point defects and Cd in non-polar ZnCdO films

Year: 2013

Version: Final published version

On the interplay of point defects and Cd in non-polar ZnCdO films

A. Zubiaga, F. Reurings, F. Tuomisto, F. Plazaola, J. A. García, A. Yu. Kuznetsov, W. Egger, J. Zúñiga-Pérez, and V. Muñoz-Sanjosé

Articles you may be interested in

Defect-dependent carrier transport behavior of polymer:ZnO composites/electrodeposited CdS/indium tin oxide devices
J. Appl. Phys. **118**, 044503 (2015); 10.1063/1.4927520

Thermal evolution of defects in undoped zinc oxide grown by pulsed laser deposition
J. Appl. Phys. **116**, 033508 (2014); 10.1063/1.4890460

Determination of secondary ion mass spectrometry relative sensitivity factors for polar and non-polar ZnO
J. Appl. Phys. **110**, 094906 (2011); 10.1063/1.3660417

Photoluminescence spectroscopy and positron annihilation spectroscopy probe of alloying and annealing effects in nonpolar m -plane ZnMgO thin films
Appl. Phys. Lett. **96**, 151904 (2010); 10.1063/1.3394012

Postgrowth annealing of defects in ZnO studied by positron annihilation, x-ray diffraction, Rutherford backscattering, cathodoluminescence, and Hall measurements
J. Appl. Phys. **94**, 4807 (2003); 10.1063/1.1609050

On the interplay of point defects and Cd in non-polar ZnCdO films

A. Zubiaga,[1] F. Reurings,[1] F. Tuomisto,[1] F. Plazaola,[2] J. A. García,[3] A. Yu. Kuznetsov,[4] W. Egger,[5] J. Zúñiga-Pérez,[6] and V. Muñoz-Sanjosé[7]

[1]*Department of Applied Physics, Aalto University, P.O. Box 11100, 00076 Aalto, Espoo, Finland*
[2]*Elektrizitatea eta Elektronika/Fisika Aplikatua II Sailak, Euskal Herriko Unibertsitatea, Posta Kutxatila 644, 48080 Bilbao, Spain*
[3]*Fisika Aplikatua II Saila, Euskal Herriko Unibertsitatea, Posta Kutxatila 644, 48080 Bilbao, Spain*
[4]*Department of Physics, University of Oslo, P.O. Box 1048 Blindern, NO-0316 Oslo, Norway*
[5]*Inst. für Angewandte Physik und Messtechnik, Univ. der Bundeswehr München, 87755 Neubiberg, Germany*
[6]*CRHEA CNRS, F-06560 Valbonne, France*
[7]*Dept. de Fisica Aplicada i Electromagnetisme, c/ Doctor Moliner 50, E-46100 Burjassot (Valencia), Spain*

Non-polar ZnCdO films, grown over m- and r-sapphire with a Cd concentration ranging between 0.8% and 5%, have been studied by means of slow positron annihilation spectroscopy (PAS) combined with chemical depth profiling by secondary ion mass spectroscopy and Rutherford back-scattering. Vacancy clusters and Zn vacancies with concentrations up to $10^{17}\,cm^{-3}$ and $10^{18}\,cm^{-3}$, respectively, have been measured inside the films. Secondary ion mass spectroscopy results show that most Cd stays inside the ZnCdO film but the diffused atoms can penetrate up to $1.3\,\mu m$ inside the ZnO buffer. PAS results give an insight to the structure of the meta-stable ZnCdO above the thermodynamical solubility limit of 2%. A correlation between the concentration of vacancy clusters and Cd has been measured. The concentration of Zn vacancies is one order of magnitude larger than in as-grown non-polar ZnO films and the vacancy cluster are, at least partly, created by the aggregation of smaller Zn vacancy related defects. The Zn vacancy related defects and the vacancy clusters accumulate around the Cd atoms as a way to release the strain induced by the substitutional Cd_{Zn} in the ZnO crystal. © 2013 American Institute of Physics. [http://dx.doi.org/10.1063/1.4775396]

I. INTRODUCTION

ZnO has attracted much attention lately due to its outstanding optoelectronic properties in the ultraviolet energy range.[1] The band-gap of CdO is only 2.16 eV at room temperature and by adding Cd to ZnO, the band-gap of the alloy can be tuned in a wide energy range. In $Zn_{0.93}Cd_{0.07}O$ films grown by pulser laser deposition, a band-gap of 3.0 eV has been reported, down from 3.28 eV in pure ZnO.[2] Still, there is a big widespread in the band-gap values measured by optical absorption[2,3] or photoluminescence.[4] The low solubility of Cd (the thermodynamical limit is 2%) remains the main problem to overcome before homogeneous ZnCdO films necessary for technological applications can be built. The large ionic radius of Cd^{2+} (92 pm), as compared to 74 pm of Zn^{2+}, increases the elastic energy of the alloyed lattice. In addition, the different coordination number of Cd in rocksalt CdO and Zn in wurtzite ZnO affects the electrostatic energy of Cd_{Zn}. The phase diagram of the ZnO-CdO system is not yet well understood[5] and the formation of domains is difficult to avoid.[4] Alloys with Cd fraction up to 70% have been obtained[3,5–7] where rocksalt CdO domains are not created. In metal-organic vapor phase epitaxy (MOVPE), non-polar ZnCdO films up to 8.5% of Cd can be introduced before domains with different Cd contents are observed in high resolution X-ray diffraction (HRXRD) measurements.[8] Nevertheless, in MOVPE ZnCdO thin films grown over c-sapphire with a ZnO/GaN template, the formation of nanodomains of wurtzite ZnCdO with different Cd fractions has been reported.[9]

In non-polar ZnCdO films, the problems due to the polar character of Zn(Cd)O,[10,11] like spontaneously generated electric fields or the increased concentration of defects near the interface with the substrate, are avoided.[8,12] In this work, the effect of introducing Cd in non-polar MOVPE ZnO films grown over m- and r-plane sapphire with Cd atomic fractions ranging up to 5% is studied by means of slow positron annihilation spectroscopy (SPAS) and a combination of Rutherford backscattering spectroscopy (RBS) and secondary ion mass spectroscopy (SIMS). SPAS is specially well suited for the study of acceptor type vacancies in thin films and SIMS in combination of RBS is capable to measure the Cd depth profile in detail, specifically in the vicinity of the ZnCdO/ZnO buffer interface.

II. EXPERIMENTAL

Non-polar ZnCdO samples were grown at 380 °C using a MOVPE reactor operated at atmospheric pressure. Part of the alloyed films were deposited on r- sapphire (R0, RB1, RB2), while the rest were deposited over m-sapphire substrates (M0, MB1, MB2, MB3) without any previous chemical or thermal treatment. Films R0 and M0 were deposited directly over the sapphire substrate, while films MBx and RBx were deposited over a ZnO buffer layer of around 800 nm in order to prevent the appearance of zinc blende ZnCdO phases or pure CdO domains. In addition, a ZnO film of around $1\,\mu m$ was deposited over r-sapphire. Films grown over r-sapphire have a-plane $[11\bar{2}0]$ orientation, while

the films grown over m-sapphire have m-plane [10$\bar{1}$0] orientation.[13] A HRXRD measurement of the $2\theta \sim 56.6°$ peak corresponding to [11$\bar{2}$0] in ZnCdO grown over r-sapphire shows that more than one phase with different Cd contents coexist when [Cd] > 8.5%, while in samples with lower Cd content the existence of domains could not be observed. The peak corresponding to the phase with higher Cd content is wider (full width half maximum (FWHM) = 0.45°), an indication that it has lower crystalline quality. More details about the growth process can be found in Ref. 8.

The SIMS intensity versus sputtering time was measured employing a Cameca IMS7f microanalyzer. An area of $125\,\mu m \times 125\,\mu m$ was bombarded with 10 keV O_2^+ ions and Cd^+ ions were collected from the middle of the crater. The depth of the crater was measured with a Dektak 8 profilometer and the measurement depth was obtained assuming a constant erosion rate. Cd concentration values were calibrated by RBS employing 2 MeV He^+ ions backscattered into a 170° direction relative to the incident beam direction. The Cd content in the plateau and the main features of the films are resumed in Table I.

Slow positron Doppler broadening experiments were performed at room temperature with a monoenergetic positron beam using energies between 0.5 and 38 keV.[14] The Doppler broadening of the annihilation radiation was detected with two Ge detectors of 1.35 keV resolution in the annihilation peak. The data were analyzed using the conventional S and W parameters, defined as the fractions of counts in the central (S, $|E_\gamma$-511 keV$| \leq 0.8$ keV) and the "wing" (W, 2.9 keV $\leq |E_\gamma$-511 keV$| \leq 7.4$ keV) parts of the annihilation line. The normalized S and W parameters were obtained using the values in a ZnO reference sample without acceptor type vacancies (S = 0.42, W = 0.073). More information about the experimental setup can be found in Ref. 14.

Positron lifetime measurements were performed using a pulsed positron monoenergetic beam working in the 0.5–18 keV energy range at room temperature.[15] The full width half maximum of the pulse was 150 ps and the resolution function was composed by three Gaussians. The annihilation radiation was collected with a BaF_2 detector coupled to a fast photomultiplier.[15] More than 10^6 events were collected in each spectrum. The lifetime spectra were decomposed using three lifetimes (n(t)= $\sum I_i/\tau_i \exp[-t/\tau_i]$).

TABLE I. Distribution of Cd and vacancy clusters within the samples: sample name, Cd RBS concentration, thickness of the samples (film + buffer) estimated from SPAS, thickness of the Cd plateau and thickness of the Cd enriched region, including the low Cd content tail. All thickness values are given in μm. Samples R0 and M0 are without buffer.

Sample label	[Cd] (%)	Film thickness	Cd plateau	Overall Cd enriched
R0	3.5	1.0	0.9	1.1
M0	3.5	0.9	0.5	1.0
RB1	1.2	1.7	0.8	1.1
RB2	5.0	1.9	1.1	1.5
MB1	0.8	2.0	0.8	1.3
MB2	3.5	2.4	1.2	2.3
MB3	5.0	2.3	1.1	2.2

The longest one corresponds to the annihilation of the positronium created mainly in the surface, while other two come from annihilation inside the sample. The concentration of the main positron traps has been estimated fitting the experimental data to a two defect trapping model.[14] The positron average lifetime $\tau' = \tau - I_3\tau_3$ (the average lifetime where the longest component has been subtracted) and τ_1 are

$$\tau' = \tau_b + \frac{\kappa_v(\tau_v - \tau_b) + \kappa_{cl}(\tau_{cl} - \tau_b)}{\lambda_b + \kappa_v + \kappa_{cl}}, \qquad (1)$$

$$\tau_1 = \frac{1}{\lambda_b + \kappa_v + \kappa_{cl}}\left[1 + \kappa_v\tau_v\left(1 + \frac{\kappa_{cl}}{\lambda_b - 1/\tau_{cl} + \kappa_v}\right)\right], \quad (2)$$

where $\lambda_b = 1/\tau_b$ is the inverse bulk lifetime and κ_v and κ_{cl} are the trapping rates of the Zn vacancies τ_v and the vacancy clusters τ_{cl}, respectively. The trapping rates κ are related to the defect concentration $[V]$ through the relation $\kappa_v = \mu_v[V]/N_A$, where $N_A = 8.3 \times 10^{22}$ cm^{-3} is the particle density of ZnO and μ_v is the trapping coefficient of the defect.

The S and W parameters inside the buffer have been obtained from the experimental S and W parameters using a model of implantation and annihilation of slow positrons in semiconductor heterostructures with short positron diffusion length[16] to subtract the contribution from the ZnCdO film. The samples have been divided into three regions: the ZnCdO film, the ZnO buffer, and the sapphire substrate, and the annihilations parameters are assumed to be constant within each region. Monoenergetic positrons are implanted according to a Makhovian profile which depends on the kinetic energy of the positrons and the mass density of the sample. The positron distribution at the annihilation moment is well approximated by the implantation profile when the diffusion length of positrons can be neglected. The annihilation parameters for positrons of certain energy are the weighted sum of the parameters of each region, where the weights are given by the probability of annihilation in each region. To avoid any influence coming from positrons annihilating in surface states, the parameters of positrons with implantation energies lower than 5 keV are not included in the fitting.

III. RESULTS AND ANALYSIS

A. SIMS

The SIMS measurements of the ZnCdO films are shown in Figure 1. Most Cd forms a plateau with a concentration of $\sim 10^{21}$ cm^{-3} within the ZnCdO film with a thickness ranging between 0.5 and 1.2 μm. The Cd concentration in the plateau of each sample is proportional to the mean Cd concentration. The sample having the lowest Cd concentration, MB1, also has the lowest Cd concentration in the plateau, while, samples RB2 and MB3 have the largest Cd content and the higher concentration value on the plateau also. The plateau finishes 0.8–1.2 μm before the buffer-substrate interface, in good agreement with the buffer thickness ($\sim 0.8\,\mu m$). In the samples grown over r-sapphire (a-ZnO), the plateau reaches the end of the ZnCdO film while in the samples grown over
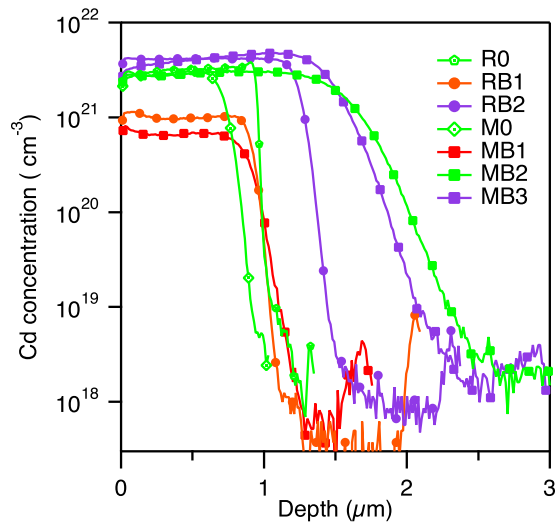
FIG. 1. SIMS results showing the Cd distribution within the ZnCdO film + ZnO buffer samples.

m-sapphire (m-ZnO) the plateau ends ∼0.35–0.4 μm before the end of the film.

At larger depths, the Cd concentration drops abruptly till it reaches ∼10^{18} cm^{-3}. The tail region extends 0.3–1.3 μm in the samples with substrate. Knock-on effects during the SIMS measurement are negligible and they do not affect the shape of the tail. The effective diffusion length of Cd has been estimated to be 0.1–0.2 μm and it is dominated by the interdiffusion of Cd and Zn during the growth of the film.[17] The length of the tail correlates with the thickness and the growth time of the ZnCdO films, indicating that the diffusivity of Cd beyond the plateau is the same in a-ZnO and m-ZnO. In samples without buffer, R0 and M0, Cd cannot enter the sapphire substrate and the Cd tail is shorter (0.1–0.4 μm). In these samples, the Cd plateau reaches the substrate (R0) or finishes at ∼0.35 μm from the substrate (M0).

B. Doppler broadening PAS

Figure 2 shows the S and W positron parameters of the ZnCdO films, the bulk reference ZnO and the MOVPE ZnO film versus the positron implantation energy. At implantation energies lower than 5 keV, a fraction of the positrons diffuses back and annihilates in surface states resulting in high S and low W parameters. At energies larger than 15 keV, the positron parameters in the reference sample are almost constant and equal to the bulk value (S = 0.42, W = 0.073). In the MOVPE a-ZnO film, the S parameter is also approximately constant between 5 keV and 15 keV (S = 0.44), while the W parameter shows a bump at W = 0.063 which corresponds to positrons annihilating in Zn vacancy related defects with a concentration of 7×10^{17} cm^{-3}. At energies higher than 14 keV, positrons start to annihilate in the sapphire substrate (thickness d ∼ 1.4 μm) and the positron parameters decrease till their value in sapphire (S = 0.407, W = 0.060).

The positron diffusion length in the ZnCdO films, estimated from the fraction of positrons with E < 5 keV diffusing back and annihilating in surface states,[14] ranges between 20 and 30 nm, typical values for ZnO films. Positrons annihi-
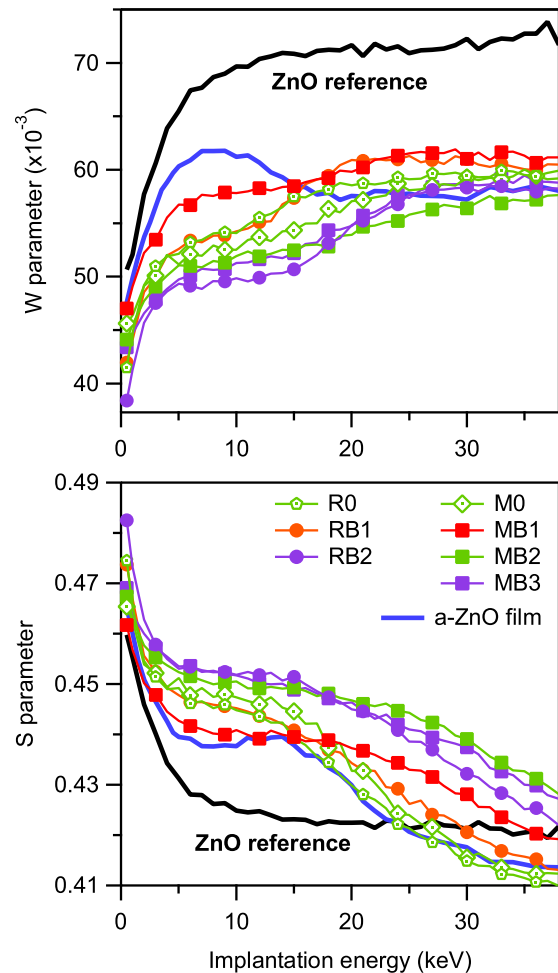

FIG. 2. W and S parameter of the alloyed samples (line with markers) represented versus the positron implantation energy in the upper and lower left panels, respectively. A bulk ZnO reference sample (black line) and the nonpolar MOVPE ZnO film grown over r-sapphire (blue line) are also shown. The labels of the lower and the upper panels are equal.

lating with energies between 5 and 15 keV have S parameters larger than S = 0.439, the value of Zn monovacancies,[18] in all samples except MB1. W parameters are also lower than the corresponding values for the Zn monovacancy (W = 0.058). The high (low) S (W) parameter values within the ZnCdO films are due to annihilation at vacancy clusters of larger open volume than the isolated Zn monovacancy. The size of the vacancy clusters will be estimated below during the discussion of the slow positron lifetime results. The film with the lowest Cd content, MB1, has also the lowest S parameter, comparable to the value of the ZnO film, and its W parameter is the highest among the ZnCdO films. Moreover, in MB1, the concentration of vacancy clusters is the lowest among the ZnCdO films and a larger fraction of positrons gets trapped in smaller Zn vacancy related defects.

Positrons with implantation energies larger than 15 keV partly annihilate inside the ZnO buffer. The S parameter decreases steadily, while the W parameter increases indicating that the concentration of clusters is lower inside the buffer. The main positron traps are, instead, Zn vacancies related defects with an open volume similar to the isolated Zn vacancy. Between 20 and 28 keV, positrons start to annihilate in the sapphire substrate. The W parameter saturates at

0.055–0.06, while S parameter continues decreasing gradually as more positrons annihilate in sapphire.

To rule out that the high (low) S (W) parameter is due to the formation of positronium, the Doppler spectra of sample RB2, which has the highest Cd and vacancy clusters content, have been decomposed using ACARFIT.[19] Two Gaussian components of 3 and 5 keV FWHM have been found which can be related to annihilation with valence electrons and core electrons, respectively. A very narrow component (≤ 1.5 keV) coming from the self-annihilation of para-Positronium[20] has not been found.

Figure 3 shows the normalized W versus the normalized S parameter of the ZnCdO film for all the measured samples. The value of the Zn vacancy (V_{Zn}) and its vacancy line is also given for reference. The vacancy line joins the V_{Zn} and the ZnO bulk value (1.0/1.0) and when the Zn vacancies are the main positron trap, the W/S values lie over it. Contrarily, the W/S values within the ZnCdO film (filled coloured symbols in Figure 3) and the ZnO bulk sample lie over a different line (dashed red line). The W/S values lying over the second line correspond to samples where positrons get trapped in a single type of vacancy clusters. The vacancy clusters of the ZnCdO films have lower W parameter than the vacancy clusters created in ZnO hydrothermal bulk samples irradiated with N$^+$ (Ref. 21) and the MBE ZnO films irradiated with O$^+$ (Ref. 18) (see Figure 3).

The S and W parameters within the ZnO buffer in samples RBx and MBx have been obtained from the experimental values using the positron implantation and annihilation model explained in Sec. II. This is justified since the positron diffusion length $\sim$20–30 nm is much smaller than the typical thickness of the sample ($\sim$1 μm). The thickness of the

samples (film + buffer) has been estimated as twice the mean implantation depth at the largest implantation energy before positrons start to annihilate in the substrate[16] (see Table I). The thickness of the ZnCdO film has been estimated subtracting the thickness of the buffer. Finally, the thickness of the substrate has been assumed to be infinite. The W/S values (inset of Figure 3) lie over the Zn vacancy line indicating that within the ZnO buffer, where the Cd concentration is several orders of magnitude lower, the main positron traps are Zn vacancy related defects. Probably, there are also some vacancy clusters, specially in the region close to the interface with the ZnCdO film, but at a lower concentration than inside the film. In samples RB1, MB1, and MB2, where the Cd content is lower, the W/S values lie closer to the bulk value while the W/S values of samples RB2 and MB3, which have the highest Cd content, are closer to the Zn vacancy value and they are comparable to the value in the ZnO film.

C. Lifetime PAS

The positron lifetime inside the ZnCdO film has been measured for samples RB2 and MB2 using monoenergetic positrons with implantation energies between 0.5 and 18 keV. The average lifetime of positrons with the lowest implantation energy is long (≥ 400 ps) due to the contribution from positrons annihilating in surface states and positronium formed in the surface, but it decreases steadily as less positrons back-diffuse to the surface. At implantation energies between 5 and 15 keV, the average lifetime remains approximately constant at $\sim$270 ps in both samples. The spectra have been decomposed into three components after subtracting an appropriate source component composed by three Gaussians.[15] The longest lifetime component τ_3 (1–3 ns, not shown) is related to the pick-off annihilation of positronium in the surface and positrons in surface states. Its intensity is maximum for low energy positrons and it decreases till its background value ($\sim$1%-2%) at energies larger than 5 keV.

Figure 4 shows the positron lifetime results after subtracting the longest lifetime component from the average lifetime, $\tau' = \tau - \tau_3 I_3$, the average lifetime of positrons is $\sim$255–260 ps. In the sub-surface region, at depths below 0.1 μm (mean implantation depth $\bar{z} = 0.05$ μm, $E \leq 3$ keV), τ' increases up to 300 ps due to incomplete separation of the long lifetime. The second lifetime component, $\tau_2 \sim 350$–400 ps, corresponds to annihilation in the vacancy clusters.

Its lifetime is around 2–2.4 times longer than in the bulk (170 ps). The ratio to the bulk lifetime is related to the size of the vacancy clusters. For monovacancies in semiconductors, its value ranges around 1.2–1.3, while it is higher for vacancy clusters. Vacancy clusters are estimated to be formed by 4–5 V_{Zn}-V_O missing pairs by comparing to lifetime ratios in SiC, where they were thoroughly studied.[22,23] Vacancy clusters with a lifetime of 340 ps have been previously observed in bulk ZnO samples.[24] Its intensity remains approximately constant in both ZnCdO films (E $\sim$ 5–15 keV) around 40%–60%. On the other side, τ_1 has a value of $\sim$200–210 ps and it is a mixture of annihilation in Zn vacancy related defects ($\sim$230 ps) and in the bulk.
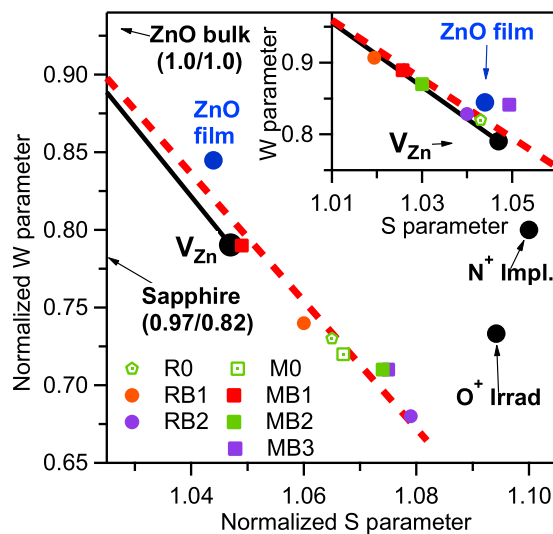

FIG. 3. Normalized W versus S parameters in the ZnCdO film of all the measured samples. W/S values of the Zn vacancy,[18] the vacancy clusters measured in N$^+$ implanted hydrothermal ZnO,[21] and O$^+$ irradiated MBE films[18] are given for reference. The Zn vacancy line extending between the Zn vacancy and the ZnO bulk values is drawn and the values of the sapphire substrate and the ZnO bulk, which lie out of the graph, are indicated by arrows. The dashed red line joins the W/S values in the ZnCdO film and the ZnO bulk value. The inset figure shows the normalized W/S values in the buffer layer for samples RBx and MBx. The W/S value of the ZnO film is given for reference in the main graph and the inset.
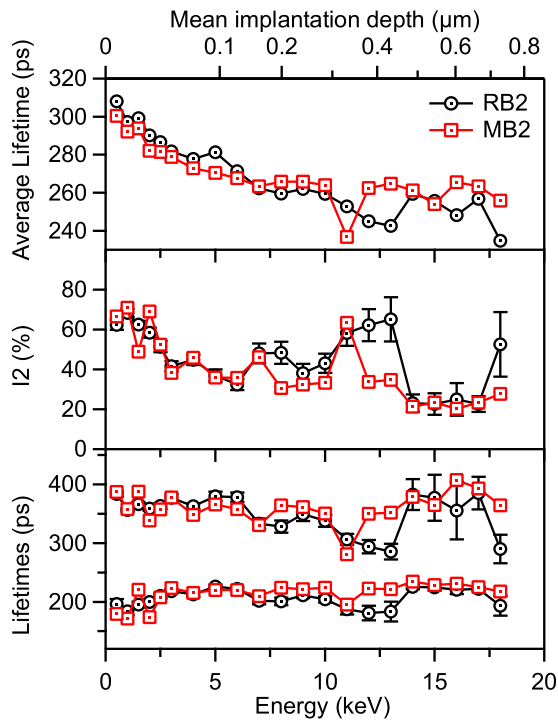
FIG. 4. Slow positron lifetime spectroscopy results for samples RB2 (black dotted circles) and MB2 (red dotted squares). τ' (upper panel), I_2 (middle panel), τ_2 and τ_1 (lower panel) are shown versus the positron implantation energy. The top axis shows the corresponding mean implantation depth of the positrons.

The concentration of Zn vacancies $[V_{Zn}]$ and vacancy clusters $[V_{cl}]$ in the ZnCdO films has been estimated using the two defect trapping model of Eqs. (1) and (2). For the trapping coefficient of the Zn vacancy, a typical value for semiconductors at room temperature $\mu_v = 2 \times 10^{15}$ cm^{-3} (Ref. 14) has been used while for the vacancy clusters is larger $\mu_{cl} \sim N \times \mu_v = 10^{16}$ cm^{-3}. The trapping rates fitted from the experimental data are $\kappa_v \sim 2 \times 10^{10}$ s^{-1} and $\kappa_{cl} \sim 10^{10}$ s^{-1}. The corresponding concentration of vacancy clusters ($[V_{cl}] \sim 10^{17}$ cm^{-3}) is one order of magnitude lower than the concentration of vacancies ($[V_{Zn}] \sim 10^{18}$ cm^{-3}) inside the ZnCdO film, and around 4 orders of magnitude lower than the concentration of Cd. Still, the fraction of positrons trapped in the vacancy clusters remains high due to their large trapping coefficient.

IV. DISCUSSION

Figure 5 shows that the S parameter within the ZnCdO film, a good measure of the content of vacancy clusters, correlates well with the Cd content. The content of vacancy clusters is maximum within the ZnCdO film where the concentration of Cd is $\sim 10^{21}$ cm^{-3}. When the concentration of Cd decreases below 10^{21} cm^{-3}, smaller Zn vacancy related defects become the main positron trap. In the buffer, where [Cd] is more than 2 orders of magnitude smaller than within the plateau, the Zn vacancy related complexes are the main positron traps.

The scheme of Figure 6 shows that the depth distributions of the high [Cd] plateau (the region above the red full line) and the positrons annihilating with high S parameter
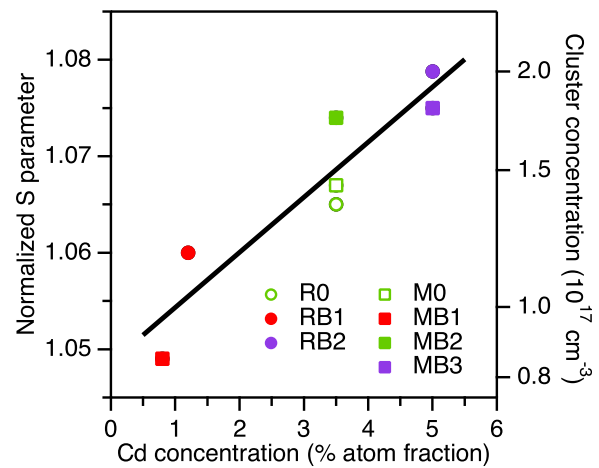

FIG. 5. Normalized S parameter in the ZnCdO film versus the Cd content. The line represents a linear fit to the data. The corresponding concentration of vacancy clusters is represented in the right axis.

(dark blue region) agree in the samples with buffer (RBx and MBx). The [Cd] plateau finishes about 0.4 μm before the end of the m-ZnCdO film while in a-ZnCdO reaches till the end of the film. The high stability of the surface of m-ZnO[25] makes more difficult the incorporation of Cd into the m-ZnO buffer. On the other side, the length of the Cd tail is proportional to the thickness of the ZnCdO film, and its growth time, in both m-ZnCdO and a-ZnCdO. The Cd tail is formed by diffusion of Cd towards the substrate during the growth of the film and no differences have been observed in the diffusion of Cd in m-ZnO and a-ZnO.

In samples M0 and R0, the spatial distribution of the vacancy clusters does not follow the same trend. In R0, the
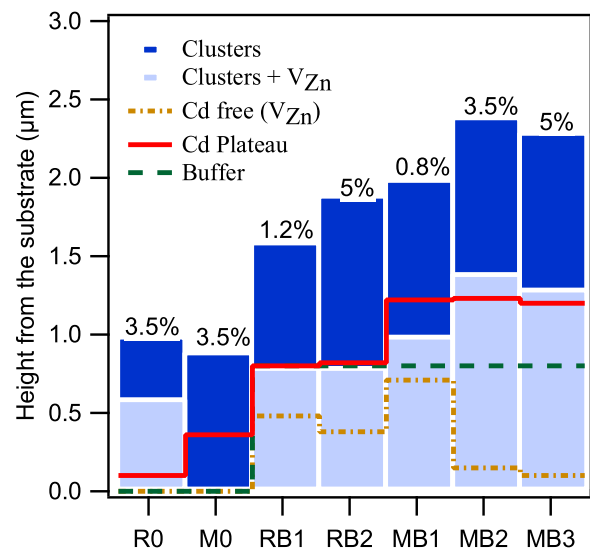

FIG. 6. Schematics of Cd, vacancy clusters, and Zn vacancy depth distribution in all samples. The zero value of the height corresponds to the position of the interface between the substrate and the buffer (RBx and MBx) or the substrate and the film (R0 and M0). The dark blue region represents the region where the concentration of vacancy clusters is the largest. In the light blue region, the Zn vacancy related defects are the main positron trap. The point-dashed orange line marks the limit of the Cd distribution. The red full line marks the limit between the high Cd region near the surface and the Cd tail region. The dashed green line at 0.8 μm marks the interface between the ZnCdO film and the ZnO buffer in samples RBx and MBx.

Cd plateau is $\sim$1 μm and it reaches the interface with the substrate, but the region with the highest vacancy clusters is restricted to a region $\sim$0.4 μm near the surface. At longer depths, the content of vacancy clusters decreases although the S (W) parameter remains higher (lower) than the value of the isolated Zn vacancy(S > 1.05, W < 0.78). Distinctly, in sample M0, the content of vacancy clusters remains high ($\sim 10^{17}$ cm^{-3}) in the whole ZnCdO film while the plateau with high [Cd] is confined to the first 0.5 μm. Differences in the distribution of acceptor type vacancies near the interface with the substrate have been observed in films of ZnO[26] and GaN[27] depending on the growth polarity and the lattice mismatch. In the samples with a buffer layer, the strain is absorbed near the interface with the substrate and the defects do not propagate into the ZnCdO layer. On the other side, in the samples without buffer, the defects created near the interface effects near the substrate affect the distribution of vacancy clusters within the film.

A. Zn vacancies

The concentration of Zn vacancy related defects increases from $\sim 10^{17}$ cm^{-3} inside the buffer up to $\sim 10^{18}$ cm^{-3} inside the ZnCdO film when the concentration of Cd is $\sim 10^{21}$ cm^{-3}. The background value in the buffer is comparable to the concentration in the non-polar a-ZnO grown over r-sapphire.

It should be noted that the isolated Zn vacancies are mobile already at 600 K.[28] The Zn vacancies measured in as-grown samples must form complexes[24,29] with another intrinsic defect or impurity or they must be stabilized at dislocations or grain/domain boundaries. The lifetime and the Doppler broadening parameters of the resulting complex are typically similar to the isolated Zn vacancy. The main candidate to form complexes with Zn vacancies are O vacancies. The O vacancy has a very small open volume and it has a donor nature so it does not trap positrons when it is isolated. But, V_{Zn}-nV_O can form stable complexes similar to the ones observed in InN.[30] The positron annihilation properties of the resulting defect complex would be similar to the isolated Zn vacancy.

B. Vacancy clusters

The concentration of vacancy clusters within the Cd plateau ($\sim 10^{17}$ cm^{-3}, $10^{-4} \times$ [Cd]) is proportional to the Cd content. Doppler broadening results show that they are the same type in all films independently of the Cd concentration being above or below the 2% thermodynamical limit and they are composed by 4–5 V_{Zn}-V_O vacancy pairs. Beyond the Cd plateau, their concentrations decrease fast and smaller Zn vacancy related defects remain as the main positron trap. The local distortion of the ZnO crystal around the Cd_{Zn} ion can induce the formation of Zn and O vacancies which can merge and form vacancy complexes. The aggregation of Zn vacancy related defects has been observed in irradiated samples when the concentration of Zn vacancies is $\sim 2 \times 10^{18}$ cm^{-3}.[18]

Doppler results show that the as-grown vacancy clusters in ZnCdO films differ from the vacancy clusters introduced

after irradiating ZnO with O ions[18] or N ions[21] specially in the W parameter. The S and W parameters for positrons annihilating in the vacancy clusters (saturated trapping) have been estimated using the annihilation fractions ($\eta_{V_{Zn}} = 0.49$, $\eta_{V_{Cl}} = 0.35$) obtained from the lifetime experiments. The S parameter S = 1.14–1.16 is 15% larger than in the bulk and 10% than in Zn vacancies, while the W parameter W = 0.38-0.47 is 50%-60% lower than in the bulk and 40%-50% lower than in the Zn vacancies. It is also lower than the W parameter in other vacancy clusters formed in irradiated samples and N$^+$ implanted samples. This is in apparent contradiction with the high atomic number of Cd and indicates that a strong local rearrangement must occur when forming the vacancy clusters around the Cd atom which avoids that the positron annihilates with electrons from Cd. The Doppler broadening results suggest that the chemical environment is similar to the Zn vacancy related defects measured in as-grown samples, and the higher (lower) S(W) parameter is related to an increase of the open volume.

C. Interplay of defects and Cd

The equilibrium concentration of Zn vacancy type defects in as-grown ZnO films is typically one order of magnitude lower than in the ZnCdO films. They are mobile at relatively low temperature (600 K) and in as-grown samples they form complexes with other point defects, extended defects or impurities. The high concentration of Zn vacancies in ZnCdO shows that samples have a high concentration of other point(O vacancies) or extended defects (dislocations, grain/domain boundaries). The vacancy cluster is introduced, at least partly, by the agglomeration of smaller Zn vacancy related defects. They are created only when [Cd] is $\sim 10^{21}$ cm^{-3}, an indication that the vacancy clusters are created when the strain of the material is large. It should be noted that the vacancy clusters are created even when the concentration of Cd is below the thermodynamical limit.

Cd is preferentially incorporated to ZnO in substitutional position of Zn (Cd_{Zn}). It has a large ionic radius (92 pm) compared to Zn (74 pm) and its oxide (CdO) crystallizes in the cubic rocksalt structure (coordination number 6), instead of the hexagonal wurtzite of ZnO (coordination number 4). This increases the elastic and electrostatic energy and induces a strain in the ZnO crystal which is accommodated by the creation of structural defects or the creation of nano-domains with different Cd concentrations.[9] The accumulated strain will end up in the sample not being homogeneous any more when the Cd concentration increases above 8.5%.

V. CONCLUSIONS

Homogeneous non-polar ZnCdO films with Cd concentration ranging between 0.8%, below the thermodynamical saturation limit of 2%, and 5% have been studied by means of slow positron annihilation spectroscopy combined with chemical depth profiling by SIMS/RBS. Most Cd stays inside the ZnCdO film but while the high Cd concentration plateau reaches the interface with the buffer and the substrate in a-ZnO, it ends $\sim$0.4 μm before in m-ZnO. This difference has been linked to the high stability of the surface in m-ZnO.

On the other side, Cd diffuses up to 1.3 μm towards the ZnO buffer during the growth of the film but no differences have been found for the diffusion of Cd in a-ZnO and m-ZnO. The dominant vacancy type acceptor is vacancy clusters with a concentration up to $10^{17}\,cm^{-3}$ and Zn vacancies with concentrations of $10^{18}\,cm^{-3}$. A correlation has been measured between the content of Cd and vacancy clusters within the ZnCdO film when the concentration is $\sim 10^{21}\,cm^{-3}$. When [Cd] decreases, the concentration of vacancy clusters decreases strongly and smaller Zn vacancy related defects become the main positron trap. Within the buffer, when [Cd] $<10^{18}\,cm^{-3}$, the concentration of vacancy clusters is negligible and the concentration of Zn vacancy related defects is similar to the values measured in non-polar ZnO films. The vacancy clusters are composed by 4–5 missing V_{Zn}-V_O vacancy pairs and they are created, partially at least, by agglomeration of smaller Zn vacancy related defects. They show a strong rearrangement of the open volume around the Cd atom. Zn vacancy related defects are stable complexes involving probably a single Zn vacancy and, at least, one O vacancy. The high concentration of Zn vacancy related defects and vacancy clusters is linked to the strain induced by Cd in ZnO crystal. It is an indication of the existence of a high concentration of dislocations or nanodomains in non-polar ZnCdO even when [Cd] is below the thermodynamical saturation limit.

ACKNOWLEDGMENTS

[1]A. Tsukazaki, A. Ohtomo, T. Onuma, M. Ohtani, T. Makino, M. Sumiya, K. Ohtani, S. F. Chichibu, S. Fuke, Y. Segawa, H. Ohno, H. Koinuma, and M. Kawasaki, Nature Mater. **4**, 42 (2005).

[2]T. Makino, Y. Segawa, M. Kawasaki, A. Ohtomo, R. Shiroki, K. Tamura, T. Yasuda, and H. Koinuma, Appl. Phys. Lett. **78**, 1237 (2001).

[3]D. W. Ma, Z. Z. Ye, and L. L. Chen, Phys. Status Solidi A **201**, 2929 (2004).

[4]K. Sakurai, T. Takagi, T. Kubo, D. Kajita, T. Tanabe, H. Takasu, S. Fujita, and S. Fujita, J. Cryst. Growth **237–239**, 514 (2002).

[5]V. Venkatachalapathy, A. Galeckas, M. Trunk, T. Zhang, A. Azarov, and A. Yu. Kuznetsov, Phys. Rev. B **83**, 125315 (2011).

[6]J. Ishihara, A. Nakamura, S. Shigemori, T. Aoki, and J. Temmyo, Appl. Phys. Lett. **89**, 091914 (2006).

[7]S. Sadofev, S. Blumstengel, J. Cui, J. Puls, S. Rogaschewski, P. Schafer, and F. Henneberger, Appl. Phys. Lett. **89**, 201907 (2006).

[8]J. Zuñiga Pérez, V. Muñoz-Sanjosé, M. Lorenz, G. Benndorf, S. Heitsch, D. Spemann, and M. Grundmann, J. Appl. Phys. **99**, 023514 (2006).

[9]F. Bertram, S. Giemsch, D. Forster, J. Christen, R. Kling, C. Kirchner, and A. Waag, Appl. Phys. Lett. **88**, 061915 (2006).

[10]U. Özgur, Y. Alivov, C. Liu, A. Teke, M. Reshchikov, S. Dogan, V. Avrutin, S. J. Cho, and H. Morko, J. Appl. Phys. **98**, 041301 (2005).

[11]A. Zubiaga, F. Tuomisto, F. Plazaola, K. Saarinen, J. A. García, J. F. Rommeluere, J. Zuñiga Pérez, and V. Muñoz-Sanjosé, Appl. Phys. Lett. **86**, 42103 (2005).

[12]J. Zuñiga Pérez, V. Muñoz-Sanjosé, E. Palacios-Lidón, and J. Colchero, Phys. Rev. Lett. **95**, 226105 (2005).

[13]J. Zuñiga Pérez, V. Muñoz-Sanjosé, E. Palacios-Lidón, and J. Colchero, Appl. Phys. Lett **88**, 261912 (2006).

[14]K. Saarinen, P. Hautojärvi, and C. Corbel, "Positron annihilation spectroscopy of defects in semiconductors," *Semiconductors and Semimetals* (Academic, New York, 1998), p. 209.

[15]F. Reurings, F. Tuomisto, W. Egger, B. Lowe, L. Ravelli, S. Sojak, Z. Liliental-Weber, R. E. Jones, K. M. Yu, W. Walukiewicz, and W. J. Schaff, Phys. Status Solidi A **207**, 1087 (2010).

[16]A. Zubiaga, J. A. García, F. Plazaola, F. Tuomisto, J. Zuñiga Pérez, and V. Muñoz-Sanjosé, Phys. Rev. B **75**, 205305 (2007).

[17]A. Yu. Azarov, T. C. Zhang, B. G. Svensson, and A. Yu. Kuznetsov, "Cd diffusion and thermal stability of CdZnO/ZnO heterostructures," Appl. Phys. Lett. **99**, 111903 (2011).

[18]A. Zubiaga, F. Tuomisto, V. A. Coleman, H. H. Tan, C. Jagadish, K. Koike, S. Sasa, M. Inoue, and M. Yano, Phys. Rev. B **78**, 035125 (2008).

[19]P. Kirkegaard, N. J. Pedersen, and M. Eldrup, *PATFIT-88: A Data-Processing System for Positron Annihilation Spectra on Mainframe and Personal Computers* (Roskilde, Denmark, 1989).

[20]W. Brandt, G. Coussot, and R. Paulin, Phys. Rev. Lett. **23**, 522 (1969).

[21]T. M. Børseth, F. Tuomisto, J. S. Christensen, E. V. Monakhov, B. G. Svensson, and A. Y. Kuznetsov, Phys. Rev. B **77**, 045204 (2008).

[22]G. Brauer, W. Anwand, P. G. Coleman, J. Störmer, F. Plazaola, J. M. Campillo, Y. Pacaud, and W. Skorupa, J. Phys.: Condens. Matter **10**, 1147 (1998).

[23]R. Aavikko, K. Saarinen, F. Tuomisto, B. Magnusson, N. T. Son, and E. Janzén, Phys. Rev. B **75**, 085208 (2007).

[24]A. Zubiaga, F. Plazaola, J. A. García, F. Tuomisto, V. Muñoz-Sanjosé, and R. Tena-Zaera, Phys. Rev. B **76**, 085202 (2007).

[25]U. Diebold, L. V. Koplitz, and O. Dulub, Appl. Surf. Sci. **237**, 336 (2004).

[26]A. Zubiaga, F. Tuomisto, J. Zuñiga Pérez, and V. Muñoz-Sanjosé, Acta Phys. Pol. A **114**, 1457 (2008).

[27]F. Tuomisto, T. Paskova, R. Kröger, S. Figge, D. Hommel, B. Monemar, and R. Kersting, Appl. Phys. Lett. **90**, 121915 (2007).

[28]F. Tuomisto, K. Saarinen, D. C. Look, and G. C. Farlow, Phys. Rev. B **72**, 085206 (2005).

[29]F. Tuomisto, A. Mycielski, and K. Grasza, Superlatt. Microstruct. **42**, 218 (2007).

[30]C. Rauch, I. Makkonen, and F. Tuomisto, Phys. Rev. B **84**, 125201 (2011).